

DESIGN AND OPTIMIZATION OF MULTI-QUANTUM WELLS FOR  
GaAs BASED VERTICAL CAVITY SURFACE EMITTING LASERS

by

FARAH Z. JASIM

Thesis submitted in fulfillment of the requirements  
for the degree of  
Doctor of Philosophy

September 2010

## **ACKNOWLEDGMENTS**

“All praises and thanks to ALLAH”

I would like to express my sincere gratitude to my main supervisor Dr. Khalid M. Omar for his valuable guidance and dedicated support throughout this project, without his patience, guidance and constant supports, this work would not have been possible. I also would like to sincerely thank our Dean and my co-supervisor Professor Dr. Zainuriah Hassan, for her creative guidance, intellectual support and simulating discussions. Her valuable advice in many matters is highly appreciated. Thanks also to the offices of Universiti Sains Malaysia, Institute of Postgraduate Students, both Deputy Deans and all the staff in the main office. The friendship and assistance from the students at NOR laboratory are also appreciated.

I would like to give my great honor and warmest thanks to my parents for their prayers, unlimited support and true love had maimed the geographical distances between us. Finally, great thanks from my heart to my lovely husband and our children Tania and Yosif, for their understanding, patience and support throughout the period of my research.

## TABLE OF CONTENTS

	Page
Acknowledgments	ii
Table of Contents	iii
List of Figures	viii
List of Tables	xv
List of Abbreviations	xvi
List of Symbols	xviii
Abstrak	xxii
Abstract	xxiv
CHAPTER 1- INTRODUCTION	1
1.1 Historical Background	2
1.2 Literature Review of GaAs Based VCSELs	3
1.3 The Choice of VCSEL Design	6
1.3.1 Etched Air Post	7
1.3.2. Ion Implanted Structure	8
1.3.3. Regrown Buried Heterostructure	9
1.3.4. Native Oxide Confinement	9
1.4 Advantages of VCSELs Structure	10
1.5 ISETCAD Software	12
1.6 Research Background	14
1.7 Research Objectives	14

1.8	Thesis Originalities	15
1.9	Out Line of Thesis	16

## CHAPTER 2- OPERATION THEORY OF VERTICAL CAVTY SURFACE

### EMITTING LASERS

2.1	Introduction	17
2.2	Absorption and Emission of Radiation	19
2.3	Quantum Well Confinement	21
2.4	VCSEL Cavity	22
	2.4.1 Single Quantum Well (SQW)	23
	2.4.2 Multi Quantum Wells (MQWs)	24
	2.4.3 Inhomogeneous Carrier Injection	25
2.5	Gain, Losses and Lasing Condition	26
2.6	Laser Rate Equations	29
2.7	Spontaneous Recombination Rate	31
2.8	Characterization of VCSELs with Quantum-Well Active Layer	32
	2.8.1 Determination of Principle Parameters	32
	2.8.2 Threshold Current Density for VCSELs with Quantum-Well Active Layer	32
	2.8.3 Differential Quantum Efficiency	35
	2.8.4 Output Light versus Input Current	37
	2.8.5 Threshold Current	38
	2.8.6 Slope of Light- Current ( $L-I$ ) Curve	40

2.9	Thermal Characteristics of VCSELs	40
	2.9.1 Influence of Temperature on Lasing Wavelength of VCSELs	41
	2.9.2 Influence of Temperature on Threshold Current and Output Power of VCSELs	43
2.10	Distributed Bragg reflectors (DBRs)	43
2.11	Transverse and Longitudinal Modes of VCSELs	46
CHAPTER 3- SIMULATOR IMPLEMENTATION		
3.1	Introduction	49
3.2	Numerical Simulation Concept	49
3.3	Physical Models	51
	3.3.1 Poisson Equation and the Electron and Hole Continuity Equations	56
	3.3.2 Quantum Well Modeling	55
	3.3.3 Carrier Capture into the Quantum Wells	56
	3.3.4 Radiative Recombination Processes in a Quantum Well	57
	3.3.4.1 Stimulated Recombination Rate	57
	3.3.4.2 Spontaneous Recombination Rate	58
3.4	Quantum Well Gain Calculations	58
3.5	Vertical Cavity Surface Emitting Lasers Simulation	58
	3.5.1 Different Grid and Structure for Electrical and Optical Problems	59
	3.5.2 The Optical Solver	60
3.6	Coupling between Optics and Electronics	60

3.7	Plot Variables Specific to VCSEL Simulation	62
3.8	Perfectly Matched Layers	62

#### CHAPTER 4- THE EFFECT OF NUMBER OF DISTRIBUTED BRAGG REFLECTORS ON VCSEL OUTPUT PERFORMANCE

4.1	Introduction	65
4.2	VCSEL Design in Numerical Simulations	66
4.3	Simulation Results and Discussion	68
4.4	Summary	75

#### CHAPTER 5- QUANTUM WELL ACTIVE REGION EFFECTS ON VCSEL PERFORMANCE

5.1	Design of VCSEL with Spacer Effect at High Performance	77
	5.1.1 VCSEL design in numerical simulations	77
5.2	Single and Multi Quantum Well(s) VCSEL Performance	87
5.3	Study Effects of Well Numbers on VCSEL Performance	87
5.4	Quantum Well Thickness on Resonant Wavelength of VCSEL	94
5.5	Summary	96

#### CHAPTER 6- DOPING CONCENTRATION AND TEMPERTURE EFFECTS ON VCSEL PERFORMANCE

6.1	Introduction	97
6.2	Analysis and Design Of VCSEL with Different Doping Concentrations	97

6.3	Analysis of Temperature Effects on the VCSEL Output Performance	108
6.4	Summary	112

CHAPTER 7- STUDY OF RADIUS SIZE EFFECTS ON VCSEL  
PERFORMANCE

7.1	Introduction	114
7.2	Simulation Results and Discussion	114
7.3	Oxide-confined aperture Effects in VCSELs	130
7.4	Summary	148

CHAPTER 8- CONCLUSIONS AND FUTURE WORK

8.1	Conclusions	150
8.2	Future Work	153

REFERENCES	154
------------	-----

PUBLICATIONS	164
--------------	-----

APPENDICES	166
------------	-----

## LIST OF FIGURES

Figure 1.1	The sample structure of VCSEL	1
Figure 1.2	Air post VCSEL structure	7
Figure 1.3	Ion implanted VCSEL structure	8
Figure 1.4	Regrown buried heterostructure VCSEL	9
Figure 1.5	Oxide aperture VCSEL structure	10
Figure 1.6	Simplified illustration of (a) an edge emitting laser and (b) 2D array of monolithic VCSEL.	11
Figure 1.7	Schematic comparing (a) the traditional and (b) TCAD based photonics design concept	13
Figure 2.1	Materials for VCSELs in wide spectral bands.	18
Figure 2.2	Energy state diagram showing different kinds of electronic transitions, the open circles represents holes and the solid circles represent electrons.	20
Figure 2.3	Quantum wells are positioned at antinodes of E field.	23
Figure 2.4	The single quantum well profile of VCSEL.	24
Figure 2.5	The multi quantum well profile of VCSEL	25
Figure 2.6	The inhomogeneous carrier injection in MQWs of VCSEL	25
Figure 2.7	Schematic of VCSEL with MQWs structure	27
Figure 2.8	Schematic diagram of MQWs with a separate confinement heterostructure	33
Figure 2.9	The dependence of threshold current density $J_{th}$ on the number of quantum wells $n_w$ with different values of reflectivity R	34
Figure 2.10	Differential quantum efficiency DQE versus reflectivity R for dielectric multilayered and Au-coated mirrors; solid lines and dashed lines represent $\alpha_{in} = 15 \text{ cm}^{-1}$ and $\alpha_{in} = 50 \text{ cm}^{-1}$ , respectively	36
Figure 2.11	Comparison of measured and calculated $L-I$ curves of VCSELs	38

Figure 2.12	Threshold current density $J_{th}$ (solid lines) and threshold current $I_{th}$ (dashed lines) against the diameter of active region $2W$ for VCSELs	39
Figure 2.13	Lasing wavelength and threshold current as a function of temperature for a 15 $\mu\text{m}$ diameter VCSEL	42
Figure 2.14	Optical gain as a function of wavelength for a 15 $\mu\text{m}$ diameter VCSEL	42
Figure 2.15	$L-I$ curves as a function of temperature for 15 $\mu\text{m}$ diameter VCSELs with resonant wavelength $\lambda_r$ of (a) 675 nm and (b) 690 nm at room temperature	43
Figure 2.16	Schematic diagram of a DBR with $m$ repeated dielectric pairs	45
Figure 2.17	A model of vertical cavity surface emitting laser VCSEL.	47
Figure 3.1	Typical design flows with DESSIS device simulation	50
Figure 3.2	Self-consistent solutions provided by ISE simulator	53
Figure 3.3	Time scale for each quantum mechanical treatment of carriers	54
Figure 3.4	Discretization of quantum well to handle the physics of quantum well transport	56
Figure 3.5	Coupling between the semiconductor transport and optics equations	61
Figure 3.6	PML coating of the structure of VCSEL	63
Figure 3.7	Naming of PML regions	64
Figure 4.1	A transverse cross-sectional view of the half portion of 850 nm GaAs/AlGaAs top surface emitting VCSEL	67
Figure 4.2	Electron carrier's density distribution inside the MQWs active region as a function of number of p-DBR pairs at temperature of 300 K	69
Figure 4.3	Hole carriers density distribution inside the MQWs active region as a function of different number of p-DBR pairs at temperature of 300 K	70
Figure 4.4	Optical material gain inside MQWs of the VCSEL structure as a function of different number of p-DBR pairs at temperature of 300 K	71
Figure 4.5	VCSEL maximum output power as a function different number of p-DBR pairs at temperature of 300 K	72

Figure 4.6	VCSEL output power as a function of injected current with different number of p-DBR pairs	72
Figure 4.7	VCSEL threshold current and threshold current density as a function of different number of p-DBR pairs	73
Figure 4.8	VCSEL slope output efficiency and differential quantum efficiency as a function of different number of p-DBR pairs	74
Figure 4.9	VCSEL mode gain as a function wavelength with different number of p-DBR pairs.	75
Figure 5.1	A schematic diagram of 850 nm GaAs/AlGaAs top surface emitting VCSEL for design A and design B, respectively	78
Figure 5.2	The energy bandgap together with electric field inside the active medium	79
Figure 5.3	The electrons and holes carrier density inside the active medium.	80
Figure 5.4	Voltage and output power as a function of the injected current for design A.	81
Figure 5.5	Laser output power of GaAs-VCSEL structure as a function of injected current for design A and design B.	82
Figure 5.6	Output slope efficiency of VCSEL structure as a function of injected current for design A and design B.	83
Figure 5.7	Differential quantum efficiency of VCSEL structure as a function of injected current for design A and design B.	84
Figure 5.8	Electron carrier's density inside the active region of the VCSEL for design A and design B.	84
Figure 5.9	Hole carrier's density inside the active region of the VCSEL for design A and design B.	85
Figure 5.10	Internal electric field of VCSEL for design A and design B.	85
Figure 5.11	Electrostatic potential of VCSEL for design A and design B.	86
Figure 5.12	Optical material gain of VCSEL for design A and design B.	86
Figure 5.13	Laser threshold current, slope efficiency, and differential quantum efficiency (DQE) as a function of well numbers	88

Figure 5.14	The electric field inside the active medium with SQW and MQWs	89
Figure 5.15	The electrostatic potential inside the active medium with SQW and MQWs	90
Figure 5.16	Electron carrier's density distribution inside the SQW and MQWs active region at temperature of 300 K	91
Figure 5.17	Hole carrier's density distribution inside the SQW and MQWs active region at temperature of 300 K	91
Figure 5.18	Optical material gain inside the SQW and MQWs active region at temperature of 300 K	92
Figure 5.19	Laser output power of SQW and MQWs GaAs active region at temperature of 300 K	93
Figure 5.20	Output slope efficiency of VCSEL structure as a function of injected current for SQW and MQWs	94
Figure 5.21	Differential quantum efficiency of VCSEL structure as a function of injected current for SQW and MQWs	95
Figure 5.22	Optical material gain spectrum for different values of quantum well thickness	95
Figure 6.1	VCSEL output power, and threshold current as a function of doping concentration.	98
Figure 6.2	VCSEL threshold current density, slope and differential quantum efficiency as a function of doping concentration	99
Figure 6.3	Energy band diagram of MQW GaAs VCSEL	100
Figure 6.4	Bandgap with optical material gain diagram of MQW GaAs VCSEL	101
Figure 6.5	Bandgap with carrier density diagram of MQW GaAs VCSEL	102
Figure 6.6	The optical intensity together with the refractive index profile.	102
Figure 6.7	Voltage and output power as a function of the injected current	103
Figure 6.8	Output slope efficiency, and output power as a function of the injected current	104
Figure 6.9	Output power and differential quantum efficiency as a function of	105

the injected current

Figure 6.10	The mode gain of proposed MQWs VCSEL as a function of wavelength	105
Figure 6.11	Near field pattern of proposed MQWs 850 nm VCSEL laser design	106
Figure 6.12	The y-cut of the near field pattern of proposed 850 nm MQWs VCSEL design	106
Figure 6.13	The far field pattern of proposed MQWs VCSEL design	107
Figure 6.14	$\theta_{//}$ and $\theta_{\perp}$ far field pattern of proposed MQWs VCSEL design	107
Figure 6.15	VCSEL maximum output power as a function of temperature.	109
Figure 6.16	VCSEL threshold current as a function of temperature	110
Figure 6.17	VCSEL slope output and differential quantum efficiency as a function of temperature	110
Figure 6.18	The output power-current characteristics of GaAs based VCSEL as a function of temperature	111
Figure 6.19	Optical mode gain as a function of wavelength.	111
Figure 7.1	The output power as a function of radius size of VCSEL	115
Figure 7.2	Electron carriers density distribution profiles inside MQWs of GaAs VCSEL	116
Figure 7.3	Hole carriers density distribution profiles inside MQWs of GaAs VCSEL	117
Figure 7.4	Optical material gain inside MQWs of GaAs VCSEL	117
Figure 7.5	Electric field distribution profiles inside MQWs of GaAs VCSEL.	118
Figure 7.6	Threshold current and maximum output power as a function of radius size of VCSEL	119
Figure 7.7	Slope efficiency and threshold current as a function of radius size of VCSEL	119
Figure 7.8	Differential quantum efficiency and threshold current as a function of radius size of VCSEL	120

Figure 7.9	(a) A transverse cross-sectional view and (b) Y-cut of transverse cross-sectional view of the half portion of MQWs 850 nm VCSEL with radius size of 2 $\mu\text{m}$ .	121
Figure 7.10	(a) A transverse cross-sectional view and (b) Y-cut of transverse cross-sectional view of the half portion of MQWs 850 nm VCSEL with radius size of 5 $\mu\text{m}$ .	122
Figure 7.11	(a) A transverse cross-sectional view and (b) Y-cut of transverse cross-sectional view of the half portion of MQWs 850 nm VCSEL with radius size of 8 $\mu\text{m}$ .	123
Figure 7.12	(a) Near field pattern and (b) Y-cut of the near field pattern of MQWs 850 nm VCSEL with radius size of 2 $\mu\text{m}$ .	124
Figure 7.13	(a) Near field pattern and (b) Y-cut of the near field pattern of MQWs 850 nm VCSEL with radius size of 5 $\mu\text{m}$ .	125
Figure 7.14	(a) Near field pattern and (b) Y-cut of the near field pattern of MQWs 850 nm VCSEL with radius size of 8 $\mu\text{m}$ .	126
Figure 7.15	(a) Far field pattern and (b) $\theta_{//}$ and $\theta_{\perp}$ far field pattern of MQWs 850 nm VCSEL with radius size of 2 $\mu\text{m}$ .	127
Figure 7.16	(a) Far field pattern and (b) $\theta_{//}$ and $\theta_{\perp}$ far field pattern of MQWs 850 nm VCSEL with radius size of 5 $\mu\text{m}$ .	128
Figure 7.17	(a) Far field pattern and (b) $\theta_{//}$ and $\theta_{\perp}$ far field pattern of MQWs 850 nm VCSEL with radius size of 8 $\mu\text{m}$ .	129
Figure 7.18	(a) A transverse cross-sectional view and (b) Y-cut of transverse cross-sectional view of the half portion of MQWs 850 nm VCSEL laser design with one upper oxide aperture.	133
Figure 7.19	(a) Near field pattern and (b) Y-cut of the near field pattern of MQWs 850 nm VCSEL with design with one upper oxide aperture.	134
Figure 7.20	(a) A transverse cross-sectional view and (b) Y-cut of transverse cross-sectional view of the half portion of MQWs 850 nm VCSEL laser design with one lower oxide aperture.	135
Figure 7.21	(a) Near field pattern and (b) Y-cut of the near field pattern of MQWs 850 nm VCSEL laser design with one lower oxide aperture.	136

Figure 7.22	(a) Far field pattern and (b) $\theta_{//}$ and $\theta_{\perp}$ far field pattern of MQWs 850 nm VCSEL design with one oxide aperture.	137
Figure 7.23	Cutaway side view of typical VCSEL optical model, showing two oxide apertures positions.	138
Figure 7.24	Variation of maximum output power with aperture diameter.	139
Figure 7.25	Variation of slope output and differential quantum efficiency with aperture diameter for the simulated VCSELs	140
Figure 7.26	Variation of threshold current with aperture diameter for the simulated VCSELs.	141
Figure 7.27	Voltage and output power as a function of the injected current for a VCSEL design with two oxide apertures.	141
Figure 7.28	Output slope and differential quantum efficiency as a function of the injected current for a VCSEL design with two oxide apertures.	142
Figure 7.29	Electron and holes carrier's density distribution inside the MQWs active region for a VCSEL design with two oxide apertures.	143
Figure 7.30	Optical material gain inside the MQWs active region for a VCSEL design with two oxide apertures	144
Figure 7.31	(a) A transverse cross-sectional view and (b) Y-cut of transverse cross-sectional view of the half portion of MQWs 850 nm VCSEL laser design with two oxide apertures.	145
Figure 7.32	(a) Near field pattern and (b) Y-cut of the near field pattern of MQWs 850 nm VCSEL laser design with two oxide apertures.	146
Figure 7.33	(a) Far field pattern and (b) $\theta_{//}$ and $\theta_{\perp}$ far field pattern of MQWs 850 nm VCSEL design with two oxide apertures	147

## LIST OF TABLES

	Page
Table 2.1 The Quantum Confinement Classification	21
Table 4.1 The Reflectivity of p-DBR	68

## LIST OF ABBREVIATIONS

2D	Two Dimensional
BPML	Bottom Perfectly Matched Layer
COD	Catastrophic Optical Damage
CW	Continuous Wave
DBR	Distributed Bragg Reflector
DQE	Differential Quantum Efficiency
EffectiveIndex	Effective Index Method
FEL	Facet Emitting Laser
FEM	Finite Element Method
FEVectorial	Finite Element Vectorial Solver Method
FFP	Far Field Pattern
FWHM	Full Width at Half Maximum
ISE	Integrated System Engineering
ISETCAD	Integrated System Engineering Technology Computer Aided Design
LAN	Local Area Network
LED	Light Emitting Diode
<i>L-I</i> curve	The output light versus input current curve
LP	Linear Polarization
LPML	Left Perfectly Matched Layer
MAN	Metropolitan Area Network
MBE	Molecular Beam Epitaxy
MQWs	Multi Quantum Wells

NEP	Near Field Pattern
OC	Oxide Confined
PML	Perfectly Matched Layer
QW	Quantum Well
RPML	Right Perfectly Matched Layer
SAN	Storage Area Network
SCH	Separate Confinement Heterostructure
SEL	Surface Emitting Laser
SFM	Single Fundamental Mode
SQW	Single Quantum Well
SRH	Shockley- Read- Hall
TCAD	Technology Computer Aided Design
TEM	Transverse Electro-Magnetic
TMM	Transfer Matrix Method
TPML	Top Perfectly Matched Layer
VCSEL	Vertical Cavity Surface Emitting Laser

## LIST OF SYMBOLS

$\Gamma_z$	Longitudinal confinement factor
$\Gamma_w$	Optical confinement of QWs
$\alpha_{in}$	Total internal loss of the laser cavity
$\alpha_{SCH}$	Absorption loss inside the SCH layers
$\Gamma_b$	Optical confinement of barriers
$\alpha_{conf}$	Scattering and absorption loss of DBR pairs
$\alpha_{diff}$	Diffraction loss
$\eta_i$	Internal quantum efficiency
$\lambda_R$	Lasing wavelength (nm)
$\tau_{ph}$	Cavity photon life time
$\Gamma$	Field confinement factor
$v_g$	Field group velocity
$\tau_n$	Carrier lifetime
$\eta_d$	Differential quantum efficiency
$\nu_R$	Lasing frequency (Hz)
$\alpha$	Absorption coefficient
$\Delta\theta$	Spreading angle
$\lambda$	Wavelength (nm)
$\phi_n$	Electron quasi-Fermi potential
$\phi_p$	Hole quasi-Fermi potential
$ \omega(x, y) ^2$	Local optical field intensity
$E_g(x)_{dir}$	Direct energy bandgap (eV)

$ M_{i,j} ^2$	Optical matrix element
$E_g(x)_{ind}$	Indirect energy bandgap (eV)
$m_e$	Electrons effective mass (kg)
$m_{lh}$	Light holes effective mass(kg)
$m_{hh}$	Heavy holes effective mass (kg)
$m_o$	Effective mass (kg)
$\theta_{  }$ and $\theta_{\perp}$	Full angle at half maximum
$\alpha_b$	Absorption loss inside the barrier layers
$A_{eff}$	Effective area
$a_n$	Differential gain
$c$	Speed of light
$d$	Thickness of the active layer ( $\mu\text{m}$ )
$E_{g,barrier}$	Energy bandgap of barrier (eV)
$E_{g,well}$	Energy bandgap of well (eV)
$G$	Modal optical gain due to stimulated emission
$g_{th}$	Threshold gain of VCSEL ( $\text{cm}^{-1}$ )
$g_n$	Gain of VCSEL at the lasing frequency ( $\text{cm}^{-1}$ )
$h$	Planck's constant ( $6.626 \times 10^{-34}$ J.s)
$I_{th}$	Threshold current (mA)
$J$	Injection current density ( $\text{A}/\text{cm}^2$ )
$J_n$	Electron current density ( $\text{A}/\text{cm}^2$ ).
$J_p$	Hole current density( $\text{A}/\text{cm}^2$ )
$J_{th}$	Threshold current density ( $\text{A}/\text{cm}^2$ )

$k_{eff}$	Effective propagation constant
$L$	Total cavity length of the VCSEL ( $\mu\text{m}$ )
$L_b$	Thickness of barriers ( $\mu\text{m}$ )
$L_w$	Thickness of the QWs ( $\mu\text{m}$ )
$m$	Number of DBR pairs
$N$	Carrier density ( $\text{cm}^{-3}$ )
$n$	Electron density ( $\text{cm}^{-3}$ )
$N_{A-}$	Number of ionized acceptors
$N_{D+}$	Number of ionized donors
$n_{eff}$	Effective refractive index of the laser cavity
$N_t$	Carrier density required to achieve transparency (population inversion).
$N_{th}$	Threshold carrier density ( $\text{cm}^{-3}$ )
$n_w$	Number of QWs
$n_b$	Number of barriers
$p$	Hole density ( $\text{cm}^{-3}$ )
$q$	Electron charge ( $1.602 \times 10^{-19} \text{ C}$ ).
$R$	Total reflectivity of DBR Pairs
$r$	Lateral distance of VCSELS
$R_1$	Top reflectivity of DBR Pairs
$R_2$	Bottom reflectivity of DBR Pairs
$R_i$	Net electron hole recombination rate
$R_{nr}$	Non-radiative emission rate
$R_{sp}$	Spontaneous recombination rate of carriers
$S_i$	Photon rate of mode

$W$	Radius of VCSEL ( $\mu\text{m}$ )
$\beta_{sp}$	Spontaneous emission factor
$\varepsilon$	Electrical permittivity
$\mu_g$	Group refractive index
$\mu_n$	Electron motility ( $\text{cm}^2/\text{V.s}$ )
$\mu_p$	Hole motility ( $\text{cm}^2/\text{V.s}$ )
$\Gamma_z$	Optical confinement factor
GaAs	Gallium arsenide

# **REKABENTUK DAN PENGOPTIMUMAN TELAGA KUANTUM BERBILANG BAGI LASER PANCARAN PERMUKAAN RONGGA TEGAK BERASASKAN**

**GaAs**

## **ABSTRAK**

Simulasi peranti bagi ciri-ciri elektrik dan optik laser pancaran permukaan rongga tegak (VCSEL) berasaskan GaAs telah diselidiki. Dalam laser sedemikian, kebocoran arus dan pemisahan lateral arus adalah beberapa masalah utama dalam rekabentuk VCSEL. Jadi dalam kajian ini, rekabentuk struktur VCSEL termasuk struktur kawasan aktif telaga kuantum berbilang (MQWs) diperihalkan dan diselidiki dengan simulasi peranti *Integrated System Engineering Technology Computer Aided Design* (ISETCAD). Parameter struktur VCSEL divariasikan dan dioptimumkan untuk prestasi tinggi. Kajian pengoptimuman ini melibatkan aspek seperti bilangan pasangan pemantul teragih Bragg (DBRs), ketebalan telaga kuantum, jumlah telaga, pendopan pasangan DBR, ciri haba dan beberapa pendekatan untuk meningkatkan dan mencapai kecekapan tinggi, arus ambang yang rendah dan kuasa output yang tinggi.

Untuk meningkatkan prestasi peranti dan mengurangkan kebocoran arus dalam rongga VCSEL, satu model baru dicadangkan di mana tiga pasang kedua-dua jenis -p dan -n DBRs yang terdekat dengan kawasan aktif, dan yang berada berdekatan dengan peruang adalah didop pada  $5 \times 10^{17} \text{cm}^{-3}$  dan yang selebihnya didop tinggi dengan kepekatan  $1 \times 10^{19} \text{cm}^{-3}$ . Dalam kes ini, padanan yang lebih baik bagi DBRs dan peruang boleh dicapai. Kuasa output sebanyak 12.7 mW, arus ambang sebanyak 280  $\mu\text{A}$ , dan voltan luar sebanyak 2.5 V diperolehi daripada struktur silinder dengan jejari 2  $\mu\text{m}$ .

Kecekapan cerun output dan dan kecekapan kuantum (DQE) adalah parameter utama bagi VCSEL. Kecekapan cerun sebanyak 0.999 dan DQE sehingga 0.683 pada panjang gelombang pancaran 848.30 nm diperolehi. Hal ini pada dasarnya adalah aspek yang sangat penting untuk dipertimbangkan bagi fabrikasi peranti.

Keluasan besar bagi rekabentuk VCSELS menghasilkan operasi mod berbilang. Satu rekabentuk baru dicadangkan untuk meningkatkan mod tunggal asas dengan operasi pada arus ambang yang rendah dengan VCSEL dua bukaan oksida terkurung (OC). Didapati apabila dua bukaan dengan jejari 4.2  $\mu\text{m}$  ditambah ke kedudukan nod gelombang pegun resonator, mod tunggal asas diperolehi serta arus ambang dikurangkan daripada 1.77 kepada 1.67 mA.

# DESIGN AND OPTIMIZATION OF MULTI-QUANTUM WELLS FOR GaAs BASED VERTICAL CAVITY SURFACE EMITTING LASERS

## ABSTRACT

Device simulations for the electrical and optical characteristics of GaAs based vertical cavity surface emitting lasers (VCSELs) have been investigated. In such lasers, carrier's leakage and lateral current separation are some of the major problems in VCSEL design. Thus, in this work the design of VCSEL structures including multi quantum wells (MQWs) active region are described and investigated by *Integrated System Engineering Technology Computer Aided Design* (ISETCAD) device simulator. The parameters of VCSEL structures are varied and optimized for high performance. This optimization study involves aspects such as the number of distributed Bragg reflectors (DBRs) pairs, thickness of quantum wells, wells number, doping of the DBR pairs, thermal characteristics and several approaches to improve and achieve high efficiency, low threshold current and high output power.

In order to enhance the device performance and reduce carrier leakage inside the VCSEL cavity, a new model is proposed where three pairs of both p and n-type DBRs nearest to the active region, and which are in the proximity of the spacer are doped at  $5 \times 10^{17} \text{ cm}^{-3}$  and the rest are doped highly at  $1 \times 10^{19} \text{ cm}^{-3}$  concentration. In this case, better matching of carrier distribution of the DBRs and the spacers can be achieved. An output power of 12.7 mW, threshold current of 280  $\mu\text{A}$ , and the outer voltage of 2.5 V were obtained from cylindrical structure with radius of 2  $\mu\text{m}$ . The output slope efficiency and differential quantum efficiency (DQE) are the key performance

parameters of the VCSEL. Slope efficiency of 0.999 and DQE up to 0.683 at an emission wavelength of 848.30 nm are achieved. This is essentially a very important aspect to be considered for the device fabrication.

Large area of VCSELS designs result in multimode operation. A new design is proposed to enhance single fundamental mode with low threshold current operation at higher output with two oxide confined (OC) apertures VCSEL. It was observed that when two apertures with radius of 4.2  $\mu\text{m}$  were added to the node position of the resonator standing wave, single fundamental mode was achieved as well as the threshold current was decreased from 1.77 to 1.67 mA.

# CHAPTER 1

## INTRODUCTION

Vertical cavity surface emitting laser (VCSEL) emits light normal to the surface of the wafer due to feedback mirrors parallel to the top and bottom surfaces of the semiconductor wafer. The cavity length of a VCSEL is very short, typically ranged from 1 to 2 wavelength of the emitted light. As a result in a single pass of the cavity, a photon has a small chance of triggering a stimulated emission event at low carrier densities (Chow et al., 1997a).

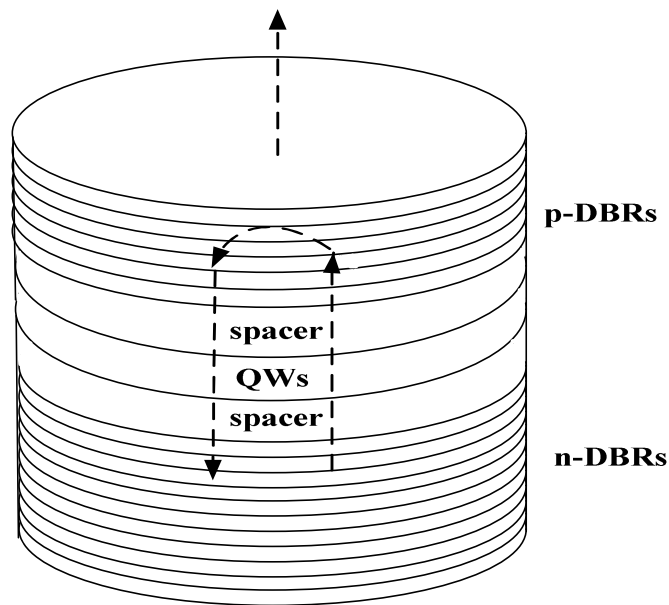


Figure 1.1: The sample structure of VCSEL.

Therefore, VCSELs require highly reflective mirrors to be efficient. In edge-emitting lasers, the reflectivity of the facets is about 30%. For VCSELs, the reflectivity required for low threshold currents is greater than 99 %. Such a high reflectivity cannot

be achieved by the use of metallic mirrors. VCSELs make use of distributed Bragg reflectors (DBRs). These are formed by laying down alternating layers of semiconductor or dielectric materials with a difference in refractive index (Wilmsen et al., 1999). The simple structure of VCSEL is shown in Fig. 1.1.

The active region usually consists of a multiple quantum well structure separated from the mirrors by spacing layers that adjust the cavity length to the lasing wavelength. Much of the work have been carried out using the GaAs/AlGaAs (Holm et al., 1999) or the InGaAs/GaAs (Kuznetsov et al., 1997) material systems, which have emission wavelengths around 850 and 1000 nm, respectively. Other material systems have been used to extend these emission wavelengths. Emission wavelengths of 1300 (Salet et al., 1997) and 1500 nm (Dias et al., 1998) have been achieved by utilizing the InGaAsP system, while red VCSELs, emitting between 650 and 670 nm, have been fabricated with the InGaAlP system (Carlsson et al., 2001). Also, research is ongoing to produce blue-green lasers utilizing the II-VI semiconducting materials.

### **1.1 Historical background**

VCSELs were at one time considered nothing more than laboratory device novelties. This attitude towards these devices in academia and in industry has changed largely due to the improvements in device performance, and the benefits of using VCSELs that have been realized. VCSELs were first pursued in 1979 by Soda et al. of TIT in Japan. They employed a double heterostructure design with a GaInAsP active region and used metallic mirrors (Soda et al., 1979). The device lased at 1.8  $\mu\text{m}$  under pulsed operation at 77 K with a high threshold. Epitaxially grown mirrors were first used in 1983 but a thick active region was employed because of a low mirror reflectivity, which still

resulted in relatively high thresholds. Advances in epitaxial technologies, in particular the development of semiconductor Bragg reflectors with extremely high reflectivities ( $\approx 0.99$ ) and the improvement in the control of thickness and composition of epitaxial layers, led to the first demonstration of continuous-wave (CW), room-temperature operation of a low-threshold VCSEL with a single-quantum well active region in 1989 (Jewell et al., 1989). Since then, rapid progress has been made in threshold reduction, two-dimensional-array fabrication (Chang-Hasnain et al., 1991), and the increase of output power (Young et al., 1993) as well as efficiency (Lear and Ctal, 1994). Further improvements in the laser structure were made with the use of ion implants (Yang et al., 1992) and natural oxide (Mitani et al., 2008 and Sharizal et al., 2009) to achieve small active regions. These improvements led to significant threshold reduction as well as better transverse mode control. In addition, the range of operating wavelengths has been extended (Koyama, 2008).

## **1.2 Literature review of GaAs based VCSELs**

The rapid progress in the development of GaAs based VCSELs is due to the promising properties of optical materials and the possibility of all monolithic structures, including the epitaxial growth of DBRs. Therefore, metal based mirrors were soon replaced by DBRs, which have been demonstrated successfully in GaAs/AlGaAs Fabry Perot microcavities. The advantages of GaAs based DBRs are (1) wide variation in refractive index between adjacent layers so that fewer layers are required to achieve high reflectivities (Chailervanitkul et al., 1985) and (2) low electrical resistance, which can be easily obtained in DBRs by using the appropriate doping profile (Lee et al., 1989 and Chalmers et al., 1993). The successful development of GaAs/AlGaAs quantum well

(QW) material for the facet emitting laser (FEL) in the late 1980s provided the solution for VCSELs. Other researchers use GaAs/AlGaAs QWs as active regions of GaAs based VCSELs (Lee et al., 1989, and Jewell et al., 1989) while others have demonstrated that GaAs/AlGaAs QWs VCSELs, incorporated with graded heterojunction interfaces into the monolithic epitaxial DBRs (Sugimoto et al., 1992), give a submilliamperere threshold current as well as CW operation at room temperature (Geels et al., 1990 a, and 1990 b).

Metal-based dielectric mirrors (i.e., such as MgF/ZnSe/MgF/Au dielectric mirror) are still used in GaAs-based 980 nm VCSELs to reduce the threshold current as well as to enhance the controllability of the optical mode (McDaniel et al., 1997). The front and the rear mirrors of this laser type are a post growth deposited MgF/ZnSe (e.g., 3.5 pairs) multilayered dielectric mirror and n-type GaAs/AlAs (e.g., 25 pairs) DBR, respectively. A  $\lambda/2$  cavity, which consists of an InGaAs QW active layer, GaAs spacers, and an oxide aperture, is sandwiched between the two mirrors. This type of device has demonstrated a threshold current of 91  $\mu$ A with an aperture diameter of 3  $\mu$ A. The use of oxide aperture is the result of the discovery of the Al-containing III-V semiconductor (Dallesasse et al., 1990). The oxide aperture is obtained by oxidizing an  $\text{Al}_x\text{Ga}_{1-x}\text{As}$  layer so that a layer of native oxide is formed. The native oxide layer has a relatively low refractive index but high electrical resistivity (Huffaker et al., 1994). Hence, a high efficiency performance due to the precise confinement of optical mode and injection current inside the active region can be achieved. It has been shown that VCSELs with front and rear AlGaAs/GaAs DBRs can also form oxide aperture inside the AlGaAs spacer layers to improve conversion efficiency (Evans et al., 1998).

The development of GaAs-based 980 nm VCSELs (i.e. using InGaAs/GaAs QWs) is based on the successful realization of 850 nm VCSELs (i.e. using

GaAs/AlGaAs QWs) as both technologies for the fabrication of DBRs are identical (i.e. InGaAs is lattice-matched with GaAs for 980 nm). A typical 980 nm oxide aperture VCSEL has 30- pairs of p-type  $\text{Al}_{0.9}\text{Ga}_{0.1}\text{As}/\text{GaAs}$  layers and 20 layer pairs of n-type DBRs of the same composition as the p-type mirrors for light emission purposes. An active layer of 3  $\text{In}_{0.2}\text{Ga}_{0.8}\text{As}/\text{GaAs}$  QWs is sandwiched between two spacer layers of AlAs from the DBRs to obtain an oxide aperture (Graham et al., 1999). 980 nm VCSEL with GaAs/AlGaAs DBRs and selective oxide configuration has demonstrated a very low threshold current (Yang et al., 1995). In addition, the maximum output power of similarly configured 980 nm VCSELs can be as large as 40 mW with an aperture diameter of only 16  $\mu\text{m}$  under CW operation at 17°C for a single mode and single lobe far field profile (Schmid et al., 1998). Furthermore, a 980 nm VCSEL array (with 19 single lasers, where each VCSEL has a 50  $\mu\text{m}$  diameter aperture arranged in honeycomb like layout to achieve maximum output power) can generate more than 1.4 W of output power under CW operation at 10°C heatsink temperature (Miller et al., 2001). It is believed that the output power of a single cavity 980 nm VCSEL will soon reach a level ( i.e. several hundred milliwatts), which is compatible with that of 980 nm high power FEL. However, multi-transverse mode operation in large aperture VCSELs is a serious problem and has to be solved in order to replace FELs. Two possible methods can be used to maintain single transverse mode operation in oxide aperture VCSELs with large cavity size: surface relief (Martinsson and Etal, 2000) and antiguiding effects in epitaxially regrown materials (Xiaofeng et al., 2006; Dharmarasu and Hillmer 2008). The basic idea of these methods is to introduce a spatial filter to eliminate the excitation of higher order transverse modes.

The rapid development of GaAs based lasers led to the commercialization of short wavelength (i.e., 850-980 nm) VCSELs in 1997 to present. Laser manufacturers sell short wavelength VCSELs with ion implantation and oxide apertures worldwide. It must be noted that reliability is one of the most important factors of commercialized VCSELs (Kashani-Shirazi et al., 2009). For example, transoceanic optical fiber communication systems based on semiconductor lasers are traditionally expected to require no more than three ship repairs in 25 years of operation (Marom, 2008; and Gan et al., 2009). For the application of short wavelength VCSELs in optical fiber computer networks such as local area networks (LANs) and metropolitan area networks (MANs), the required lifecycle should be much longer than the emergence of the next generation products. It is noted that VCSELs with oxide apertures have a long working lifetime with median time to failure of  $>10^7$  h. on the other hand, ion implanted VCSELs have an attractive selling price and acceptable reliability (Khat et al., 2010). Therefore, oxide aperture and ion implanted short wavelength VCSELs have already been installed in the most of the advanced LANs for the application in gigabit Ethernet (Alias et al., 2010a).

### **1.3 The choice of VCSEL design**

In order to effectively confine carriers in the active region and efficiently extract light from the device especially device with large active medium, different confinement schemes should be considered in the VCSELs' design. The most important technological approaches to achieve electrical and optical confinement will be presented in next paragraphs.

### 1.3.1 Etched air post

Fig. 1.2 shows the etched air post, which was the first monolithic electrically pumped VCSEL (Jewell et al., 1989).

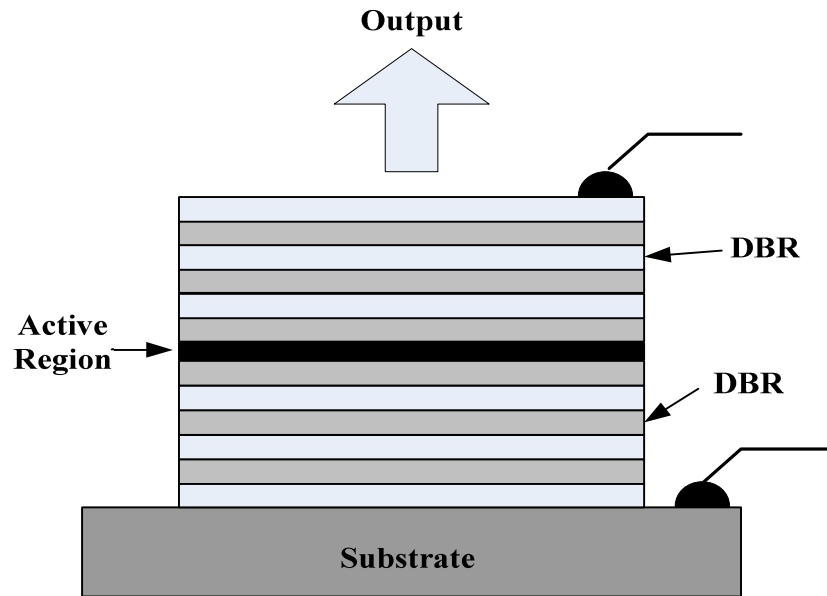


Figure 1.2: Air post VCSEL structure.

Injected carriers are forced to travel down the narrow pillar, yielding a high current density. The refractive index transition between the pillar material and the surrounding air acts as a waveguide for the radiation, confining it to the active region. This approach has suffered from a number of problems. Scattering loss from the side-walls, excess free carrier absorption at the side-walls, high ohmic resistance, poor reliability due to exposed active surface and poor heat dissipation of the structure are the main shortcomings of this approach. The latter has been improved through immersion in material with high thermal conductivity (Choquette et al., 1992). Since there is a wide lateral step, the waveguide can easily become multimode, unless the lateral dimension is

reduced. This is disadvantageous for applications (i.e. spectroscopy) requiring large, single-mode powers.

### 1.3.2. Ion implanted structure

VCSEL is fabricated using energetic protons to bombard the top DBR of the structure, destroying its electrical conductivity in selected areas Fig. 1.3 (Herrick and Petroff, 1998).

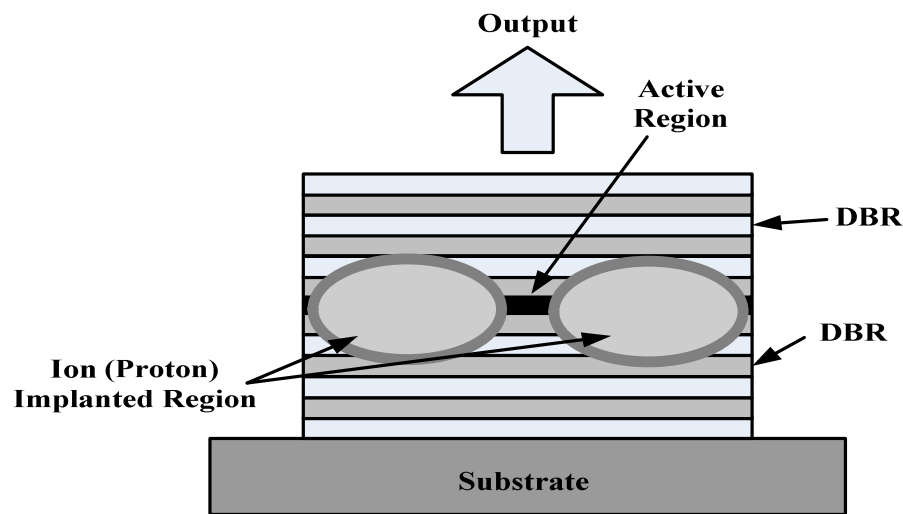


Figure 1.3: Ion implanted VCSEL structure.

As a result, the carriers are funneled into the gap defining the active region. However, the ion implantation is fuzzy at the edges and causes crystal damage in the active region, making it very difficult to define very small structures. There is no built-in waveguiding in a proton implanted VCSEL, but localized heating at the injected region induces a thermal lens by changing the refracting index. Therefore waveguiding is difficult, as the beam direction and divergence change with the temperature.

### 1.3.3. Regrown buried heterostructure

A similar structure to the air post is shown in Fig. 1.4. A pillar is etched as before, but now the gaps surrounding the pillar are filled with a semiconductor of larger bandgap. The regrown material provides electrical and optical confinement, as the refractive index is lower. The regrown region can also conduct heat away from the active region, and as the index is higher than that of air, the VCSEL can stay single-mode for longer in comparison with a simple air post. All these benefits are made at the expense of more complicated processing, which limits the usefulness of the technique in a manufacturing context.

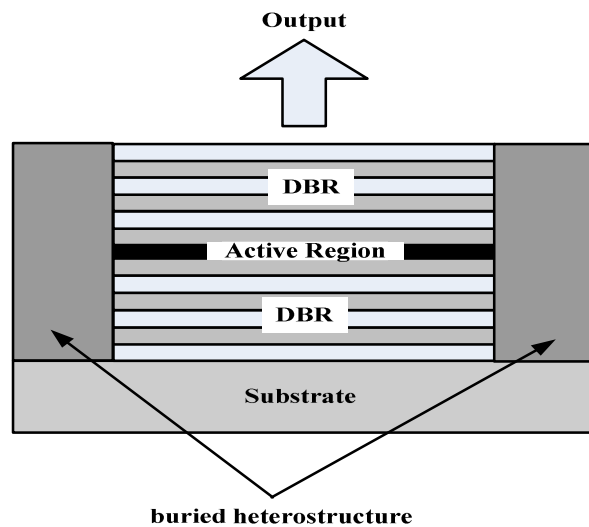


Figure 1.4: Regrown buried heterostructure VCSEL.

### 1.3.4. Native oxide confinement

The most promising technology for defining the active region is provided by the use of oxidized confinement layers as shown in Fig. 1.5. This technique makes use of the fact that AlGaAs layers with very high (>95%) aluminum content will oxidize when

exposed to water vapor at high temperatures (Tsang 1978, and Dallesasse et al., 1990). The resulting dielectric oxide has an abrupt oxidation edge. This means that very small active regions are feasible. Optical confinement is an additional advantage, which is provided by the low refractive index dielectric layer. A drawback of this technique is that the oxidation rate is very sensitive to the Al content in the oxidizing layer, a factor that may become a disadvantage in a manufacturing process. VCSELs fabricated with this technique have demonstrated efficiencies and best modulation bandwidths (Dyomin et al., 2008).

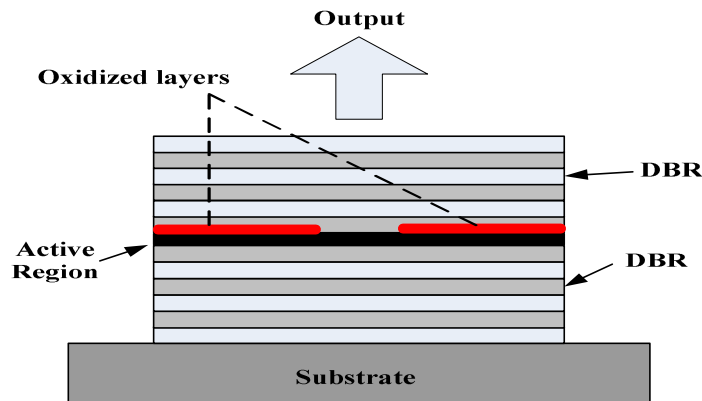


Figure 1.5: Oxide aperture VCSEL structure.

#### 1.4 Advantages of VCSELs structure

VCSELs have optical cavities orthogonal to those of conventional FELs (Lee, 1991 and Suematsu et al., 1992). This simple arrangement in the orientation of cavity significantly improves the output performance and fabrication flexibility of semiconductor lasers (Choquette and Hou, 1997). One of the main advantages of VCSELs over conventional FELs is the emitting optical beams with low divergence and a circular symmetric profile because of their wide emission surface. As a result, the

coupling efficiency to optical fiber and other optical components can be improved effectively (Chow et al., 1997a). Coupling to optical fibers is easy due to good mode matching from single mode through thick multi-mode fibers. As well as, VCSELs exhibit extremely high relaxation oscillation frequency ( $>70$  GHz) (Tauber et al., 1993) because of their short photon lifetimes. Consequently, high modulation bandwidth can be achieved. In Addition, those VCSELs facilitate wafer-scale fabrication and testing by allowing fully monolithic processes because of their vertical orientation. Therefore, the production cost and procedures for quality inspection can be reduced enormously (Chow, 1997b; Choquette and Hou, 1997).

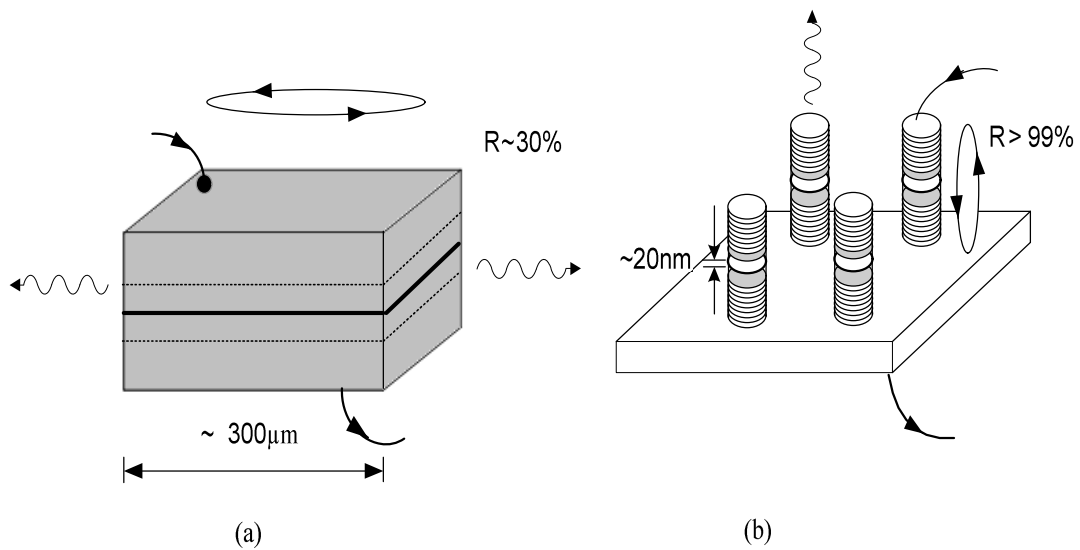


Figure 1.6: Simplified illustration of (a) an edge emitting laser and (b) 2D array of monolithic VCSEL.

High power, and low power devices are subjected to design structure and power conversion efficiency of VCSEL is greater than 50% (Siu Fung, 2003). So, ultra-low threshold operation is expected from its small cavity volume reaching milli Ampere levels (Honolyak, 1997).

VCSELs can be distinguished to three groups by the type of application (or wavelength). Firstly, short and middle range communication systems ( $\lambda \approx 800\text{-}900\text{ nm}$ ) are used for LAN (Mederer et al., 1999). Typical active region is GaAs/ AlGaAs, VCSELs working at this wavelength are the key optical source in communication systems. LAN and SAN (storage area networks) are dependent on this type of light source. Secondly, blue and UV VCSEL are used for data storage. Typical active regions are InGaN or AlInGaN ( $\lambda \approx 400\text{ nm}$ ). Latest attempts to manufacture blue VCSEL are still unsuccessful (Osinski et al., 1998a and Gan et al., 2009). Thirdly, near-IR VCSELs is used for fiber-optic communication suited for minimum of dispersion ( $\lambda \approx 1300\text{ nm}$ ) and minimum loss ( $\lambda \approx 1500\text{ nm}$ ) in fiber. Typical active region is InP-based. Recently, significant progress has been reported in 1300 nm GaInNAs VCSEL (Koyama, 2008).

### **1.5 ISETCAD software**

Traditionally, new designs of VCSEL device structures and changes to existing designs have been investigated purely experimentally; fabricating test series with parameter variations, characterizing the devices and changing the design according to the results as shown in Fig. 1.7a. Using a technology computer aided design (TCAD) software as the one presented in this work can potentially be achieved with a significantly reduced experimental effort, with drastically reduced turn-around times, and hence at lower cost Fig. 1.7b. Prior to the fabrication of a prototype, the new device design is analyzed and optimized using a simulator. Eventually, a test device is fabricated and characterized.

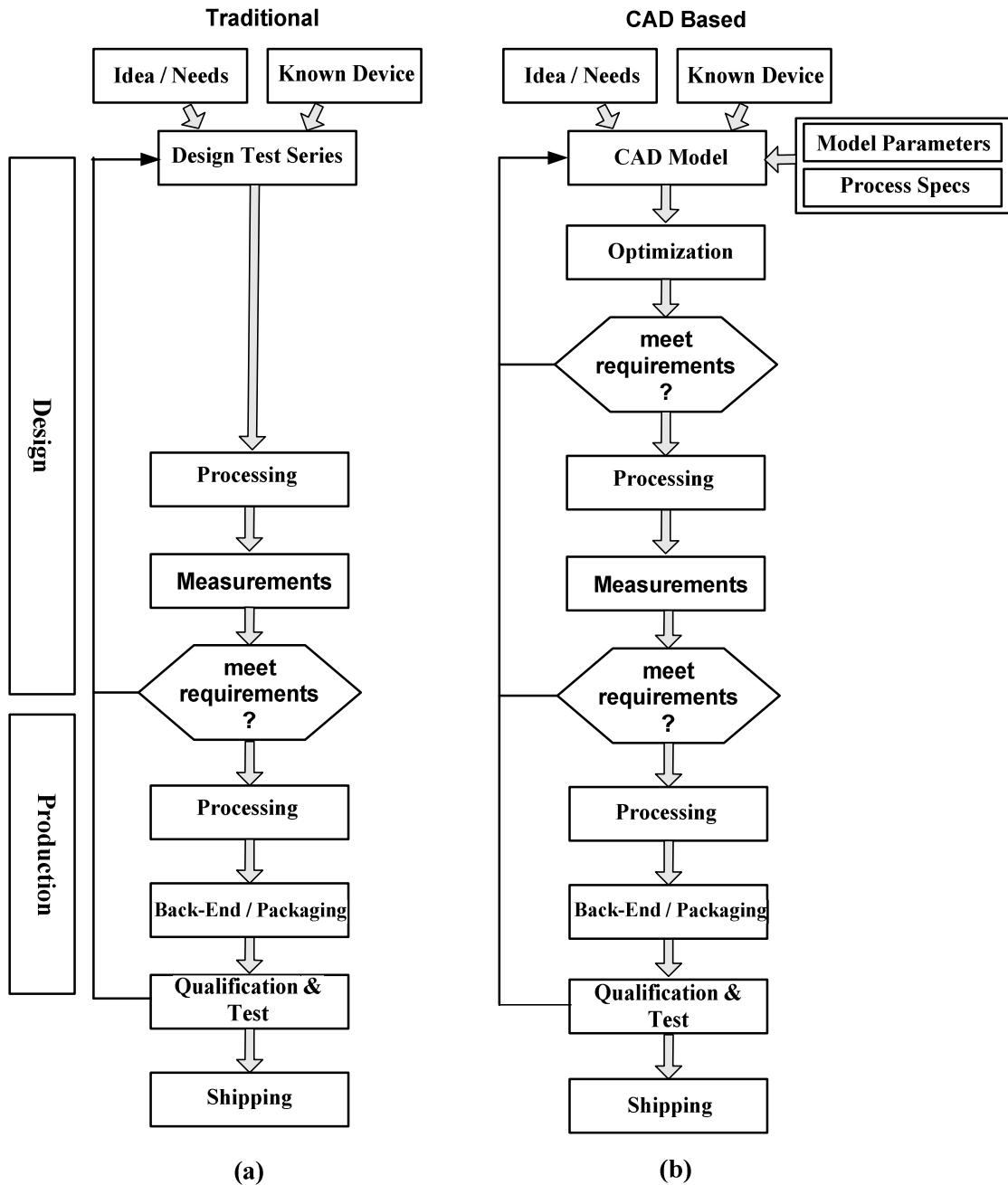


Figure 1.7: Schematic comparing (a) the traditional and (b) TCAD based photonic design concept (Streiff 2004).

The measured results are then used to correct the parameters of the model and the design procedure is restarted from the top. In addition, special test structures are used

to determine specific model parameters. In this way the accuracy of predicting device behavior is continuously improved, and the numbers of prototype fabrication cycles are lowered (Streiff 2004).

## **1.6 Research background**

The first demonstration of GaAs based 850 nm VCSEL by Iga (Iga et al., 1987) was followed by a tremendous research and developed effort around the world. Gallium arsenide VCSEL technology enables a range of applications. Examples are optical fiber computer networks such as LANs, MANs, oxide aperture and ion-implanted GaAs VCSELs have already been installed in most of the advanced LANs for application in gigabit Ethernet. However, there still remains a strong need for a more detailed understanding of microscopic physical processes in GaAs VCSELs. Advanced models and numerical simulation can help to investigate those processes and improve the device performance.

## **1.7 Research objectives**

The objectives of the simulation and theoretical research are:

1. To design GaAs VCSEL diode with low threshold current, high output power and high performance using advanced laser software simulator (ISETCAD).
2. To solve carrier's leakage and lateral current separation, which are some of the major problems in VCSEL design, because reduction of such carrier losses is important to achieve less self heating and higher output power.
3. To optimize the effect of the inhomogeneous carries distribution in multi-quantum wells.

4. To study and analyze the doping concentration of DBRs which is a crucial issue on the VCSEL output performance
5. To investigate and solve the incoherence operation of VCSEL with large active region by using the oxide apertures.

### **1.8 Thesis originalities**

Inclusion of additional two  $\text{Al}_{0.20}\text{Ga}_{0.80}\text{As}$  barriers with thicknesses of 12nm and designing the active region with four quantum wells lead to reduction of carrier losses which is important to achieve less self heating and high output power. The doping concentration also plays a critical role in increasing both the output power, radiative recombination and decreasing the threshold current. Therefore, a new design was proposed where three pairs of both p and n-type DBRs nearest to the active region, and which are in the proximity of the spacer are doped at  $5 \times 10^{+17} \text{cm}^{-3}$  and the rest are doped highly at  $1 \times 10^{+19} \text{cm}^{-3}$  concentration. In this case, better matching of carrier distribution of the DBRs and the spacers can be achieved which provide enhancement in overall performance of VCSEL.

The multimode dynamics in VCSELS was observed to be influenced by device geometry. When the active region area gets larger, the number of oscillating modes increases, producing the higher order modes. In order to effectively confine carriers in the active region and efficiently extract light from the device, a new design for VCSEL was investigated with two oxide-confined (OC) apertures which made reduction of lateral sizes of the VCSEL central active region, to enhance the single transverse fundamental mode (SFM) linear polarization ( $\text{LP}_{01}$ ) operation, and to decrease device threshold currents for the device.

## **1.9 Outline of thesis**

Briefly, the content of this thesis are presented as follows:

Chapter 1. The history of growth and the development of VCSELs different VCSELs devices and applications are presented and their advantages compared with facet emitting laser.

Chapter 2. The basic theories and concepts of VCSELs and related subjects in this work are explained.

Chapter 3. Describes the simulator itself and discusses the procedures that are involved in simulating VCSEL structure. These procedures also describe several selected models used in simulating VCSEL designs.

Chapter 4. The GaAs performance on different design structures with various distributed Bragg reflection are presented, analyzed and discussed.

Chapter 5. The GaAs performance on different design structures with single and multi quantum well(s) and the effect of additional barriers are analyzed and discussed.

Chapter 6. The effect of doping concentration on GaAs VCSEL performance is analyzed and discussed. A novel design with new doping concentration was proposed, which makes overall enhancement in VCSEL output performance.

Chapter 7. The effect of radius size of VCSEL is analyzed and discussed. A new design with two oxide confined apertures was proposed to enhance single fundamental mode with low threshold current operation at a higher output VCSEL.

Chapter 8. The outcome in this study is summarized. A few recommendations for future works also will be proposed in this chapter.

## **CHAPTER 2**

### **OPERATION THEORY OF VERTICAL CAVITY SURFACE EMITTING LASERS**

In this chapter, the simple design methodology of VCSELs under the criteria of minimum threshold current, maximum output power, slope output as well as differential quantum efficiency are described. The corresponding design equations for VCSELs with uniform gain structures are derived for the investigation. Hence, the detailed structure of lasers can be determined for optimal performance at and above the threshold operation.

#### **2.1 Introduction**

As this thesis is focused on VCSELs, we will start with some general considerations on classic, VCSELs and, more generally, with laser diodes. This chapter gives a phenomenological approach to laser diodes, emphasizing the characteristics that individualize VCSEL devices.

VCSEL diode lasers, like most other lasers, incorporate an optical gain medium in a resonant optical cavity. The design of both the gain medium and the resonant cavity are critical. The gain medium consists in a material that absorbs incident radiation over some wavelength range of interest. If it is pumped with either electrical or optical energy, the electrons within the material can be excited to higher, non-equilibrium energy levels, so the incident radiation can be amplified rather than absorbed by stimulating the de-excitation along with the generation of additional radiation. If the resulting gain is sufficient to overcome the losses of some resonant optical mode of the cavity, this mode is said to have reached threshold, and coherent light will be emitted

(Koyama, 2008). The resonant cavity provides the necessary positive feedback for the radiation being amplified, so that a lasing oscillation can be established and sustained above threshold pumping levels. As in any other oscillator, the output power saturates at a level equal to the input minus any internal losses (Denis et al., 2008). Fig. 2.1 shows some choices of materials for VCSELs.

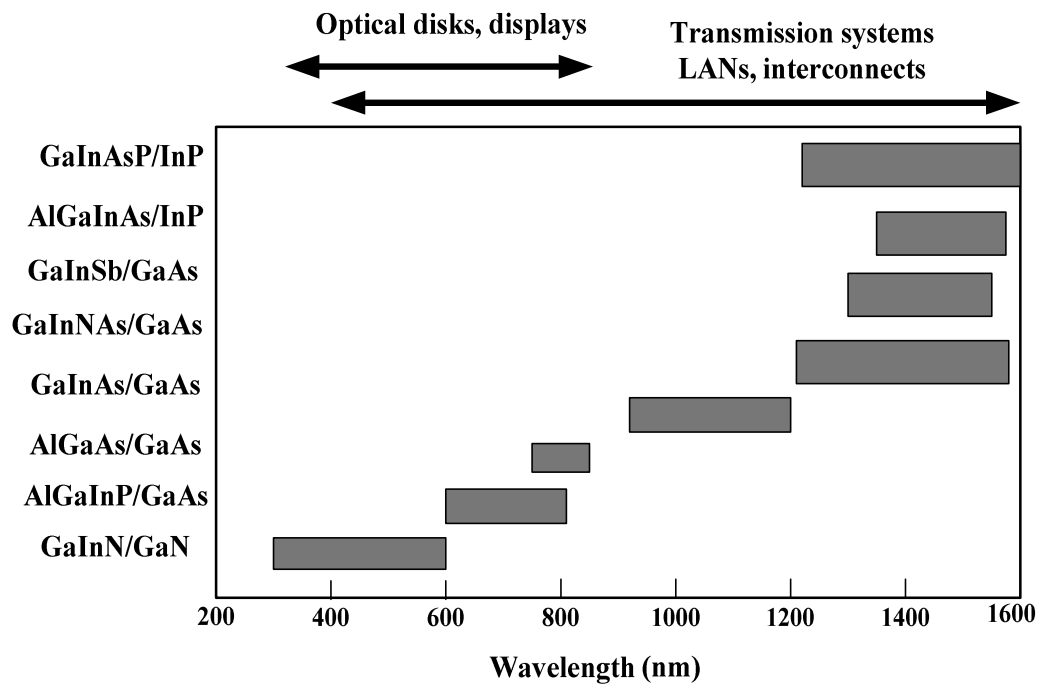


Figure 2.1: Materials for VCSELs in wide spectral bands.

Some of the problems that should be considered for making VCSELs are design of resonant cavity and mode-gain matching, using multi-layer DBRs to realize high reflective mirrors, and optical losses (such as Auger recombination, intervalence band absorption, scattering loss, diffraction loss). As well as, using of p-type doping to reduce the resistivity in p-type materials for CW and high efficiency operation. If need to form multi-layer DBRs, this will become much more severe. Heat sinking should be used for

high temperature and high power operation. COD (Catastrophic optical damage) level is very important for high power operation, and crystal growth at reasonably high temperatures (e.g., higher than half of the melting temperatures).

## **2.2 Absorption and emission of radiation**

Lasing action is a process that occurs in matter. Since matter is composed of atoms, to gain an understanding of the light-generating mechanisms within a laser, it is necessary to consider the fundamental atomic concepts. From quantum theory, atoms exist only in certain discrete states such that the absorption and emission of light causes them to make a transition from one energy state to another. Fig. 2.2 from (Tatum and Guenter, 1998) illustrates the different kinds of electronic transitions that are important.

Fig. 2.2(a) represents the transition when an electron in the conduction band recombines spontaneously with a hole in the valence band to generate a photon. This process is the primary mechanism behind the light emitting diode (LED) as the photons generated would not contribute to a coherent radiation field due to random emission time and direction.

The second process in Fig. 2.2(b) occurs when a photon is absorbed and stimulates the generation of an electron in the conduction band while leaving a hole in the valence band.

The third process in Fig. 2.2(c) occurs when an incident photon stimulates the recombination of an electron and hole, and simultaneously generates a photon. The photon generated by stimulated emission is generally of an identical energy to the one that caused it and hence the light associated with them is of the same frequency, phase

and polarization (Senior, 1992). Stimulated emission thus produces coherent radiation that ultimately gives the laser its special properties as an optical source.

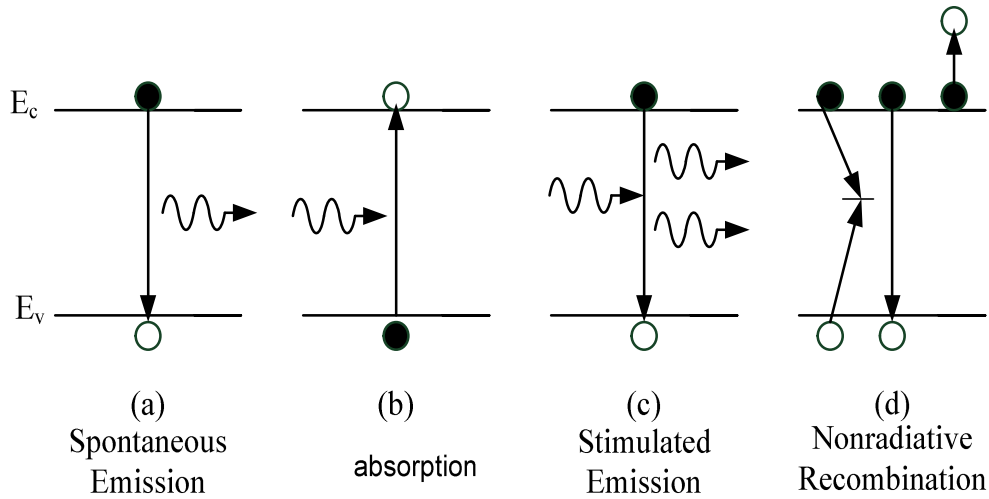


Figure 2.2: Energy state diagram showing different kinds of electronic transitions the open circles represents holes and the solid circles represent electrons (Tatum et al., 1998).

The final process in Fig. 2.2(d) represents the several nonradiative ways in which a conduction band electron can recombine with a valence band hole without generating any useful photons. The energy is dissipated as heat in the semiconductor crystal lattice and these effects are undesirable. The two general nonradiative mechanisms illustrated are nonradiative recombination centers (point defects, surfaces and interfaces) in the active region and Auger recombination. Auger recombination occurs when the electron-hole recombination energy is given to another electron or hole in the form of kinetic energy (Senior, 1992).

In order to achieve optical amplification, it is necessary to create a nonequilibrium distribution of atoms in the active medium such that the population of the upper energy level is greater than the lower energy level. If a population inversion

exists between two energy levels, the probability is high that an incoming photon will stimulate an excited atom to return to a lower state, while emitting another photon of light. The excitation mechanism (pumping) is the source of energy that raises the atoms in the active medium into their excited state, thus creating population inversion (Perchoux et al., 2008). Therefore, an understanding of these processes is an essential foundation to enter into the next section that discusses the dynamic effects of lasers by using laser rate equations.

### 2.3 Quantum Well Confinement

A quantum confinement structure is one in which the motion of electrons and holes are confined in one or more directions by potential barriers (Fox et al., 2006). The classification of quantum confinement is given in Table 2.1

Table 2.1: The quantum confinement classification

Structure	Confinement directions	Freedom directions
Quantum well	1	2
Quantum wire	2	1
Quantum dot	3	0

Quantum size effects become important when the thickness of layer becomes comparable with deBroglie wavelength of electrons or the hole in target material where quantum mechanical are expected to occur. In this case, the distribution of low energy, wave like states available for the electrons and holes confined to the active large changes

from quasi-continuous to discrete (Peter and Zory, 1993). If we consider the free thermal motion of a particle of mass ( $m$ ) in the  $z$ -direction, deBroglie wavelength at a temperature ( $T$ ) is given by (Fox et al., 2006).

$$\lambda_{de} = \frac{h}{mkT} \quad (2.1)$$

where  $k$  is Boltzman constant. The thickness can easily be obtained by molecular beam epitaxy (MBE)

## 2.4 VCSEL cavity

In new technology, most of VCSEL devices employ quantum wells within the active region. By depositing a thin layer of semiconductor with a slightly smaller band gap, one can not only define a region for recombination to occur, but also control the optical properties of the device.

Discrete energy levels are formed in the conduction and valence bands. Transitions from the conduction band to valence band energy levels occur from states that have the same value of  $n$  quantum number. The VCSEL with quantum well active region shows a number of interesting properties with characteristics that include: first, the low density of threshold current due to the small volume, and the carrier density required to achieve population inversion is small. Therefore the threshold current density of QW structures is low. (Tasang 1981a; Tasang 1981b and Alias 2010b). Second, the small variation of the threshold current with temperature (Chin et al., 1978, Hess et al., 1980, and Arakawa and Sakaki, 1982). Third, the possibility of tuning the emitted wavelength over a wide range that extended up to 100 nm, by varying the driving current. The position of the quantum wells is crucial. To maximize the gain of the

device, quantum wells should be positioned at antinodes of the E field standing wave inside the cavity as shown in Fig. 2.3.

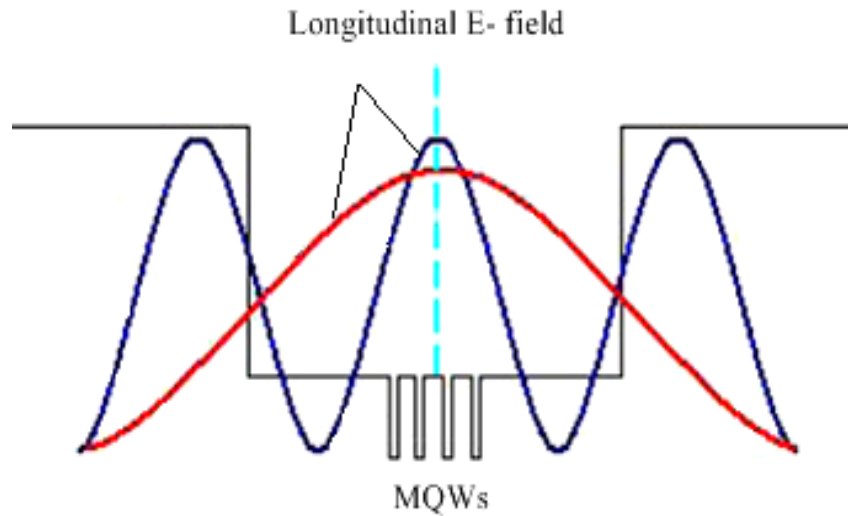


Figure 2.3: Quantum wells are positioned at antinodes of E field (Iga and Koyama, 2002).

The quantum well conception not only offers a quantitative improvement of several basic performance characteristics but also is a qualitative step in the development of VCSEL structure; the significance and implications of which are difficult to foresee at moment, but which is certainly very promising and challenges various research laboratories throughout the world to work on further development (Iga and Koyama, 2002).

#### 2.4.1 Single quantum well (SQW)

A SQW is a single layer of narrow bandgap  $E_{g,\text{well}}$  semiconductor which is sandwiched between two layers of a wider bandgap material  $E_{g,\text{barrier}}$ . Such a GaAs as a

well and AlGaAs as a barrier, where the condition  $E_{g, \text{barrier}} > E_{g, \text{well}}$  must be inquired. The following QW band diagram is obtained as shown in Fig. 2.4 (Peter and Zory, 1993).

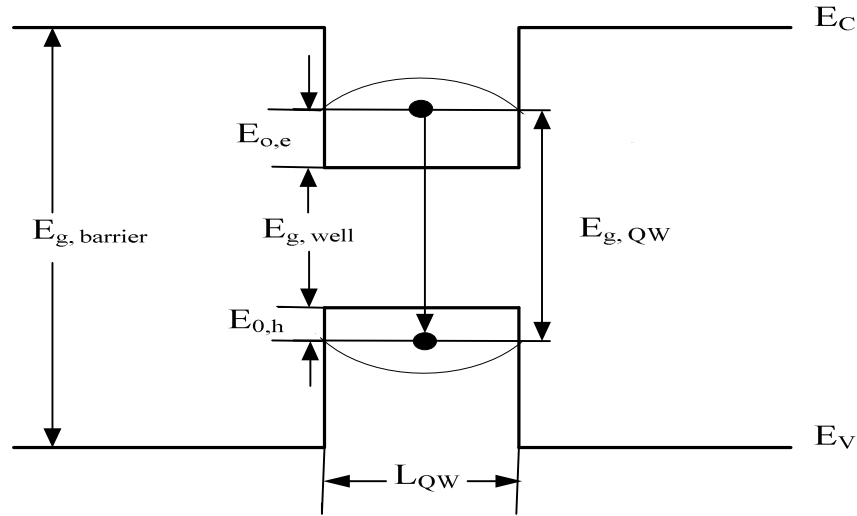


Figure 2.4: The single quantum well profile of VCSEL (Peter and Zory, 1993).

#### 2.4.2 Multi quantum wells (MQWs)

By growing a series of wells and barriers in active layer and/or cladding layer, device efficiency can be increased with the resulting structures being known as multi-quantum wells (MQWs) as shown in Fig. 2.5. Due to the quantum confinement affect the MQWs structure in the active layer results in higher gain than the normal double heterostructure and so leads to increased device efficiency; this in turn leads to increased design flexibility (Peter and Zory, 1993).

MQWs structure has more than one well, that is more carriers can be accommodated which produce lower threshold current than the SQW VCSEL that has a problem of band filling (Kasap and Capper, 2007). If SQW is filled with carriers, the luminescence saturation occurs at high current densities.

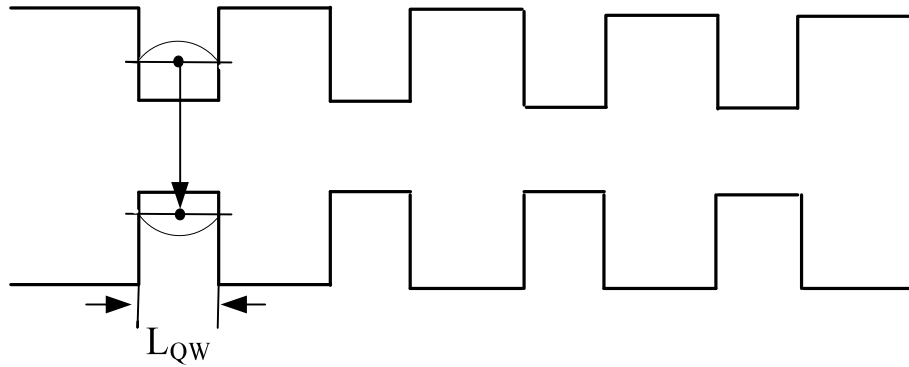


Figure 2.5: The multi quantum well profile of VCSEL (Kasap and Capper, 2007).

### 2.4.3 Inhomogeneous carrier injection

If a MQWs structure has wells separated by many thick barriers, then transport between wells will be inefficient. As a result, an inhomogeneous carrier distribution may result, which is mainly due to inefficient hole transport through the QWs caused by poor hole mobility.

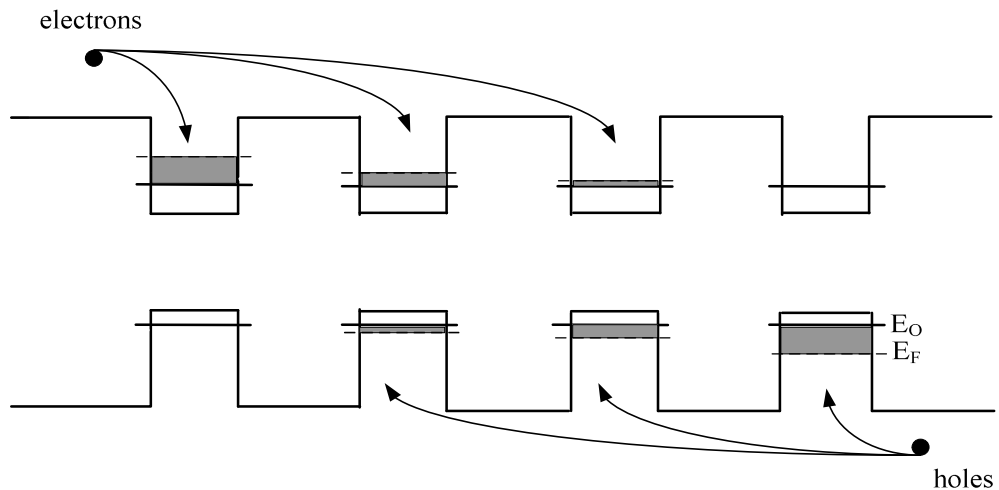


Figure 2.6: The inhomogeneous carrier injection in MQWs of VCSEL (Chang and Kuo, 2003).